J. Fluid Mech. (2020), *vol.* 894, R2, doi:10.1017/jfm.2020.289

JFM RAPIDS
journals.cambridge.org/rapids

Dual channels of helicity cascade in turbulent flows

Zheng Yan[1,2], Xinliang Li[1,2], Changping Yu[1,2,†], Jianchun Wang[3] and Shiyi Chen[3,4]

[1]LHD, Institute of Mechanics, Chinese Academy of Sciences, Beijing 100190, PR China

[2]School of Engineering Science, University of Chinese Academy of Sciences, Beijing 100049, PR China

[3]Department of Mechanics and Aerospace Engineering, Southern University of Science and Technology, Shenzhen, Guangdong 518055, PR China

[4]State Key Laboratory of Turbulence and Complex Systems, Center for Applied Physics and Technology, College of Engineering, Peking University, Beijing 100871, PR China

(Received 26 February 2020; revised 2 April 2020; accepted 8 April 2020)

Helicity, as one of only two inviscid invariants in three-dimensional turbulence, plays an important role in the generation and evolution of turbulent flows. Through theoretical analyses, we find that there are two channels in the helicity cascade process, which differs dramatically from the traditional viewpoint. In this paper, we have conducted important research on the newly proposed dual-channel helicity cascade theory, including vortex dynamic processes, intermittent discrepancies, tensor geometries, etc. The first channel mainly originates from the vortex twisting process, and the second channel mainly originates from the vortex stretching process. Antisymmetric tensors are introduced to the derivations of dual-channel helicity cascade theory, and a complex rotation frame leads to a higher helicity transfer efficiency. By analysing data from direct numerical simulations of typical turbulent flows, we find that these two channels behave differently. The ensemble averages of helicity flux in different channels are equal in homogeneous and isotropic turbulence, while they are different in other types of turbulent flows. The intermittency of the second channel is stronger than that of the first channel. In addition, we find a novel mechanism of hindered or even inverse energy cascades, which could be attributed to the second-channel helicity flux.

Key words: homogeneous turbulence, isotropic turbulence, turbulence theory

† Email address for correspondence: cpyu@imech.ac.cn

1. Introduction

Helicity exists in many natural phenomena, such as hurricanes, tornadoes and rotating 'supercell' thunderstorms in the atmosphere, Langmuir circulations in the oceans, and the α-effect and ω-effect in magnetic fields (Lilly 1986; Moffatt & Tsinober 1992). In the past few decades, there have been numerous theoretical and numerical studies indicating that helicity could reduce the aerodynamic drag and nonlinearity of Navier–Stokes equations (NSEs) and improve the mixing effectiveness of reactants (Moffatt & Tsinober 1992; Duquenne, Guiraud & Bertrand 1993). Helicity, the integral of the scalar product of velocity $\boldsymbol{u}$ and vorticity $\boldsymbol{\omega}$, is the second inviscid invariant of three-dimensional (3-D) NSEs, which indicates that helicity cascade exists in 3-D turbulent flows. Recently, new research has shown that helicity is a conservative quantity even in viscous flows (Moffatt 2017; Scheeler *et al.* 2017). Helicity is a topological variable, which measures the degree of the linkage of the vortex lines in a flow field (Moffatt 1969), and consists of linking, twisting and writhing (Moffatt 2017).

The classic Richardson–Kolmogorov–Onsager picture of 3-D turbulence is based on the concept of an energy cascade, which ignores the topology of vortices (Frisch 1995). Theoretically, there are two possibilities describing the dynamic properties of helicity and energy cascades. One is simultaneous energy and helicity cascades towards smaller scales, and the other is a pure helicity cascade with no cascade of energy, leading to broken $-5/3$ power-law solutions in turbulent magnetohydrodynamic, convective and atmospheric flows (Brissaud 1973; Kessar *et al.* 2015). Many studies have revealed through direct numerical simulations (DNS) and shell models that there simultaneously exist a transfer of energy and helicity to small scales in turbulent flows at high Reynolds number (Brissaud 1973; Waleffe 1992; Biferale 2003; Chen, Chen & Eyink 2003*a*; Biferale, Musacchio & Toschi 2013). During the joint cascade process of energy and helicity in helical turbulence, the helicity flux is more intermittent than the energy flux (Chen *et al.* 2003*b*). For rotating helical turbulence, the helicity flux dominates the direct energy cascade to small scales and the direct helicity cascade is highly intermittent (Mininni & Pouquet 2009, 2010). However, the impact of helicity on the decay rate of turbulent flows works in rotating flows, rather than in non-rotating flows (Teitelbaum & Mininni 2009).

The role of helicity in the behaviour of turbulent dynamic systems has been a controversial issue in recent decades. Previous studies have argued that the helicity cascade is carried along locally and linearly by the energy cascade and acts as a passive scalar (Andre & Lesieur 1977). Another argument insists that the helicity cascade has a dramatic effect on the energy cascade. For instance, helicity can impede the forward energy cascade and even promote the inversion of energy transfer, which could be explained as a helical bottleneck effect (Pelz *et al.* 1985; Moffatt 2014; Stepanov *et al.* 2015; Sahoo, Alexakis & Biferale 2017; Słomka & Dunkel 2017). In fact, there is always the possibility that inverse energy cascades exist when mirror symmetry is broken (Biferale, Musacchio & Toschi 2012). The theory of triadic interactions indicates that interactions with the same helicity always lead to an inverse energy cascade, which is considered a new physical mechanism for the inverse energy cascade in 3-D turbulence (Alexakis 2017; Alexakis & Biferale 2018).

Traditional theory reveals that there is only one channel of helicity cascade in turbulent flows, and that both forward and backward cascades exist in the same channel (Chen *et al.* 2003*a*; Eyink 2006; Pouquet *et al.* 2017). In turbulent flows,

vortex twisting plays a major role in the helicity cascade process (Eyink 2006). In addition, in laminar flows, the role of vortex stretching has been proven to be associated with the decrease of helicity (Moffatt & Dormy 2019). Therefore, a complete description of vortex dynamics in the helicity cascade procedure is uncertain, based on current turbulent cascade theory. In this paper, through theoretical and numerical investigations, we discover for the first time that two channels exist in the helicity cascade process. The physical mechanisms of the dual channels are totally different, and they behave differently in anisotropic turbulent flows.

The paper is organized as follows. In § 2, we propose that there exist two channels of helicity cascade, which is deduced from the NSEs. The numerical simulations are briefly described in § 3. Next in § 4, we discuss the similarities and differences of the proposed two channels in homogeneous and isotropic turbulence. The effects of the two channels on the energy cascade process are explored in § 5. Finally, conclusions will be given in § 6.

2. Derivation of dual channels in the helicity cascade

In this study, we employ the 3-D incompressible NSEs as

$$\partial \boldsymbol{u}/\partial t + (\boldsymbol{u}\cdot\nabla\boldsymbol{u}) = -\nabla(p/\rho) + \nu\nabla^2\boldsymbol{u}, \tag{2.1}$$

where $\boldsymbol{u}$ is velocity, p is pressure, ρ is density (which is constant in incompressible flows) and ν is the viscosity coefficient. To study the characteristics of the helicity cascade, we use the coarse-graining method to filter the flow field (Aluie 2011; Yu *et al.* 2013). Using a smooth low-pass filter function $G_\Delta(\boldsymbol{r})$, we can obtain the filtered physical variable such as $\widetilde{\boldsymbol{u}}(\boldsymbol{x}) = \int \mathrm{d}\boldsymbol{r}\, G_\Delta(\boldsymbol{r})\boldsymbol{u}(\boldsymbol{x}+\boldsymbol{r})$ representing the filtered velocity field on scale Δ. As mentioned above, we employ the isotropic filter in this paper. The filtered momentum equation can be deduced by making a coarse-graining operation on the above momentum equation as

$$\frac{\partial\widetilde{u}_i}{\partial t} + \widetilde{u}_j\frac{\partial\widetilde{u}_i}{\partial x_j} = -\frac{\partial\widetilde{p}}{\partial x_i} + \nu\frac{\partial^2\widetilde{u}_i}{\partial x_j\partial x_j} - \frac{\partial\tau_{ij}}{\partial x_j}, \tag{2.2}$$

where $\widetilde{u}_i$ is the filtered ith velocity component, $\widetilde{p}$ is the filtered pressure, ν is the kinematic viscosity coefficient and $\tau_{ij} = \widetilde{u_iu_j} - \widetilde{u}_i\widetilde{u}_j$ is the subgrid-scale (SGS) stress. Making a curl operation of (2.2), the following filtered vorticity equation can be obtained:

$$\frac{\partial\widetilde{\omega}_i}{\partial t} + \widetilde{u}_j\frac{\partial\widetilde{\omega}_i}{\partial x_j} = \widetilde{\omega}_j\frac{\partial\widetilde{u}_i}{\partial x_j} + \nu\frac{\partial^2\widetilde{\omega}_i}{\partial x_j\partial x_j} - \frac{\partial\gamma_{ij}}{\partial x_j}, \tag{2.3}$$

where $\widetilde{\omega}_i$ is the filtered ith vorticity component, and $\gamma_{ij} = (\widetilde{\omega_iu_j} - \widetilde{\omega}_i\widetilde{u}_j) - (\widetilde{\omega_j u_i} - \widetilde{\omega}_j\widetilde{u}_i)$ can be called as SGS vortex stretching stress, which is a newly proposed SGS tensor in this study.

Based on the above equations, the governing equations of large-scale energy $e_\Delta = \frac{1}{2}|\widetilde{\boldsymbol{u}}|^2$ and large-scale helicity $h_\Delta = \widetilde{\boldsymbol{u}}\cdot\widetilde{\boldsymbol{\omega}}$ could be easily obtained as follows:

$$\partial_t e_\Delta + \nabla\cdot\boldsymbol{J} = -\Pi_\Delta^E - 2\nu\widetilde{\boldsymbol{S}}:\widetilde{\boldsymbol{S}}, \tag{2.4}$$

$$\partial_t h_\Delta + \nabla\cdot\boldsymbol{Q} = -\Pi_\Delta^{H1} - \Pi_\Delta^{H2} - 4\nu\widetilde{\boldsymbol{S}}:\widetilde{\boldsymbol{R}}, \tag{2.5}$$

where $\widetilde{\boldsymbol{S}} = \frac{1}{2}(\nabla\widetilde{\boldsymbol{u}} + (\nabla\widetilde{\boldsymbol{u}})^{\mathrm{T}})$, $\widetilde{\boldsymbol{\Omega}} = \frac{1}{2}(\nabla\widetilde{\boldsymbol{u}} - (\nabla\widetilde{\boldsymbol{u}})^{\mathrm{T}})$ and $\widetilde{\boldsymbol{R}} = \frac{1}{2}(\nabla\widetilde{\boldsymbol{\omega}} + (\nabla\widetilde{\boldsymbol{\omega}})^{\mathrm{T}})$. Here, $\boldsymbol{J} = \widetilde{\boldsymbol{u}}|\widetilde{\boldsymbol{u}}|^2/2 + \boldsymbol{\tau}\cdot\widetilde{\boldsymbol{u}} - 2\nu\widetilde{\boldsymbol{S}}\cdot\widetilde{\boldsymbol{u}}$ denotes the space transport of large-scale energy equation,

and $\Pi_\Delta^E = -\boldsymbol{\tau} : \widetilde{\boldsymbol{S}}$ denotes the SGS energy flux. Here $\boldsymbol{Q}$ denotes the spatial transport of large-scale helicity, which is defined as

$$\boldsymbol{Q} = h_\Delta \widetilde{\boldsymbol{u}} + \widetilde{\boldsymbol{\omega}} \cdot \boldsymbol{\tau} + \widetilde{\boldsymbol{u}} \cdot \boldsymbol{\gamma} + \frac{\widetilde{p}}{\rho}\widetilde{\boldsymbol{\omega}} - \tfrac{1}{2}|\widetilde{\boldsymbol{u}}|^2\widetilde{\boldsymbol{\omega}} - 2\nu(\widetilde{\boldsymbol{u}} \cdot \widetilde{\boldsymbol{R}} + \widetilde{\boldsymbol{\omega}} \cdot \widetilde{\boldsymbol{S}}). \tag{2.6}$$

It needs to be mentioned specifically here that the first-channel helicity flux refers to Π_Δ^{H1} and the second-channel helicity flux refers to Π_Δ^{H2}. They can be expressed as

$$\Pi_\Delta^{H1} = -\boldsymbol{\tau} : \widetilde{\boldsymbol{R}}, \quad \Pi_\Delta^{H2} = -\boldsymbol{\gamma} : \widetilde{\boldsymbol{\Omega}}. \tag{2.7a,b}$$

The second-channel helicity flux is a newly defined physical quantity, and it represents the projection of the SGS vortex stretching stress on the vorticity tensor. From the definition of the first and second channels, we can find that the first channel originates mainly from the vortex twisting process (Eyink 2006), which is deduced from the filtered momentum equation, and the second channel originates mainly from the vortex stretching process, which is deduced from the vortex stretching term $\omega_i S_{ij}$. Hence, we can conclude that the helicity cascade is a combined process of vortex twisting and stretching.

Following the gradient expansion of subgrid stress (Eyink 2006), we can write the first- and second-channel helicity fluxes using the isotropic filter in the approximation forms as follows:

$$\Pi_\Delta^{H1,A} \approx \frac{\Delta^2}{12}\left\{-\mathrm{Tr}(\widetilde{\boldsymbol{R}}\widetilde{\boldsymbol{S}}^2) + \frac{1}{4}\widetilde{\boldsymbol{\omega}}^{\mathrm{T}}\widetilde{\boldsymbol{R}}\widetilde{\boldsymbol{\omega}} + \widetilde{\boldsymbol{R}} : (\widetilde{\boldsymbol{S}} \times \widetilde{\boldsymbol{\omega}})\right\}, \tag{2.8}$$

$$\Pi_\Delta^{H2,A} \approx \frac{\Delta^2}{12}\left\{\frac{1}{2}\widetilde{\boldsymbol{\omega}}^{\mathrm{T}}\widetilde{\boldsymbol{S}}\widetilde{\boldsymbol{\xi}} - \frac{1}{2}\widetilde{\boldsymbol{\omega}}^{\mathrm{T}}\widetilde{\boldsymbol{R}}\widetilde{\boldsymbol{\omega}} + \widetilde{\boldsymbol{R}} : (\widetilde{\boldsymbol{S}} \times \widetilde{\boldsymbol{\omega}})\right\}, \tag{2.9}$$

where $\widetilde{\boldsymbol{\xi}} = \nabla \times \widetilde{\boldsymbol{\omega}}$, the superscript A denotes the approximation of helicity flux, and the superscript T denotes the transpose of a matrix. The first term in (2.8) represents the inter-amplification of the strain-rate field and the symmetric vorticity gradient field; while the first term in (2.9) reflects the complicated vortex stretching dynamical process, which originates the evolutions of vorticity and vorticity gradient under the influence of the velocity strain field. This physical description of the vortex dynamical procedure of the second channel of helicity cascade is consistent with the original definition, and it provides a new vortex perspective for helicity cascade.

3. Numerical simulations

To further explore the statistical features of the dual-channel helicity cascade, we performed forced helical homogeneous and isotropic turbulence (HIT) within a cubic box with sides of length 2π with a pseudospectral solver, and the injection rates of kinetic energy and helicity are 0.1 and 0.3, respectively. The numerical simulations are carried out by solving the following incompressible NSEs:

$$\partial \boldsymbol{u}/\partial t + (\boldsymbol{u} \cdot \nabla \boldsymbol{u}) = -\nabla(p/\rho) + \nu\nabla^2\boldsymbol{u} + \boldsymbol{f}. \tag{3.1}$$

The external forcing $\boldsymbol{f}$ can be constructed by the injection rates of energy and helicity in the lowest two shells (Teimurazova *et al.* 2018). Specific parameters are summarized in table 1.

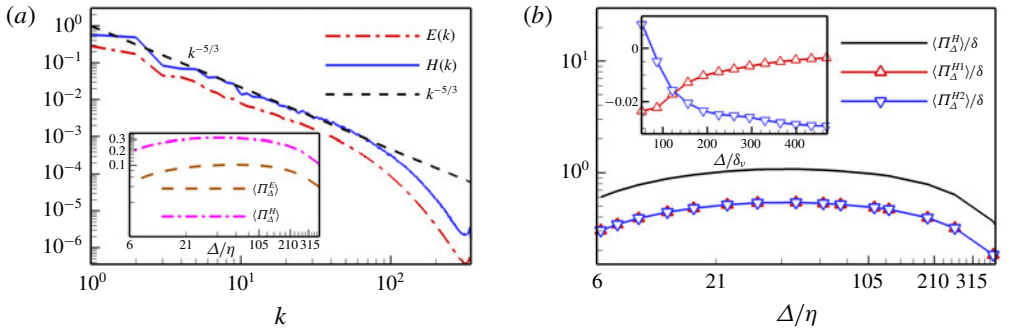

FIGURE 1. (*a*) Spectra of energy and helicity. (*b*) Ensemble averages of the first-channel, the second-channel and total helicity fluxes on the different filter widths Δ in HIT. The first-channel and second-channel helicity fluxes on the plane of $y^+ = 10$ on the different filter widths Δ in turbulent channel flows (TCF) are shown in the inset, and δ_v is the viscous length scale.

Case	Grid	Re_λ	Δ/η	λ/η	L_I/η	ϵ	δ	τ_η	T_{con}/τ_η	T_{ave}/τ_η	T_0
HIT	1024^3	341	1.52	21	102	0.10	0.30	0.054	219	30	0.338

TABLE 1. Some flow field parameters of HIT: Re_λ is the Taylor-microscale Reynolds number, Δ is the grid spacing, η is the Kolmogorov length scale, λ is the transverse Taylor microscale, L_I is the longitudinal integral length scale, ϵ is the mean kinetic energy dissipation rate, δ is the mean helicity dissipation rate, τ_η is the Kolmogorov time scale, T_{con} is the total computational time until convergence, T_{ave} is the averaging time for statistical analysis after convergence, and T_0 is the large-eddy turnover time scale. The reader can refer to Frisch (1995) for specific definitions. The numerical simulations can be considered as convergent when the viscous dissipation rates of energy and helicity are balanced with the inputting rates of energy and helicity, respectively.

The power-law solutions of kinetic energy and helicity, which ignore any intermittency corrections (Chen *et al.* 2003*a*), can be written as

$$E(k) \sim C_E \epsilon^{2/3} k^{-5/3}, \quad H(k) \sim C_H \delta \epsilon^{-1/3} k^{-5/3}, \tag{3.2a,b}$$

where C_E and C_H are Kolmogorov constants of energy and helicity, respectively. We show the ensemble averages of energy and helicity fluxes in the inset of figure 1(*a*) and the spectra of energy and helicity in figure 1(*a*). The broad regions consistent with the scaling exponent $-5/3$ of the spectra of energy and helicity, and the long plateau of energy and helicity fluxes indicate the existence of their inertial subrange in our numerical simulations.

4. Similarities and differences of the dual channels

4.1. *Equality relation*

In HIT, the ensemble averages of the first-channel and second-channel helicity fluxes are exactly equal in our numerical simulations. The equality of ensemble averages of these two channels in HIT can be proven exactly by the 3-D homogeneity condition. The detailed deductions are shown in appendix A. In figure 1, we present

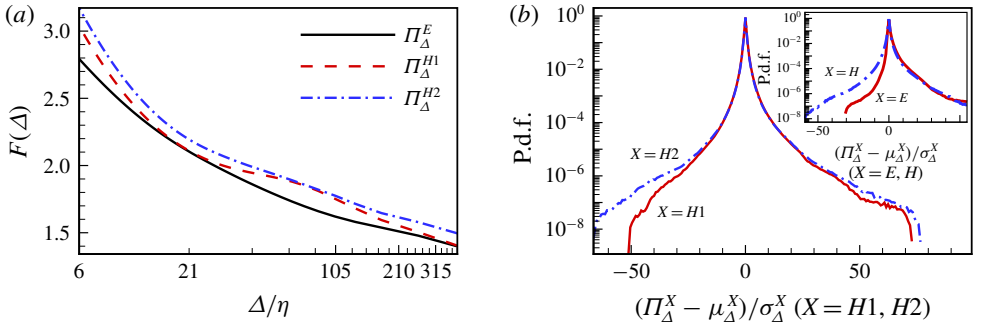

FIGURE 2. (*a*) Flatness of energy flux, and the first- and second-channel helicity fluxes. (*b*) The p.d.f.s of the first-channel helicity flux and the second-channel helicity flux with $\Delta/\eta = 24$. The p.d.f.s of energy flux and total helicity flux with $\Delta/\eta = 24$ are shown in the inset. The symbols ν and σ denote the corresponding mean and root-mean-square.

the dependences of the ensemble averages of the first-channel, second-channel and total helicity fluxes, on the different filter widths Δ, and their equality relations are numerically proven. However, the equality of these two-channel fluxes will be broken in other anisotropic flows, such as turbulent channel flows. We access the DNS data of turbulent channel flows with $Re_\tau \approx 1000$ via the Johns Hopkins Turbulence Database (Graham *et al.* 2016). The plane $y^+ = 10$ in the buffer layer was selected to typically exhibit the discrepancies of the ensemble averages of the two channels, and the isotropic filter is only employed in the horizontal directions. Their numerical results are shown in the inset of figure 1(*b*), which confirms the difference between the two channels of the helicity cascade in anisotropic turbulent flows.

4.2. *Intermittent discrepancy*

These two channels of the helicity cascade in HIT have different statistical properties in a higher statistical order. The normalized fourth-order energy flux and the first-channel and second-channel helicity fluxes are chosen to illustrate their statistical discrepancies, which are related to the intermittency representing the strong non-Gaussian fluctuations. This could be assessed quantitatively by flatness (Buzzicotti *et al.* 2018) as

$$F(\Delta) = \langle (\Pi_\Delta^X)^4 \rangle / \langle (\Pi_\Delta^X)^2 \rangle^2, \quad X = E, H1, H2. \tag{4.1a,b}$$

We exhibit the flatness of the first- and second-channel helicity fluxes and energy flux in figure 2(*a*). It is apparent that the flatness of the second-channel helicity flux is larger than that of the first-channel helicity flux, and the flatness of the first-channel helicity flux is larger than that of the energy flux over the whole scales. To further explore the discrepancy of their intermittency, we show their normalized probability density functions (p.d.f.s) at a filter width $\Delta = 24\eta$ in figure 2(*b*). Previous studies revealed that a nearly symmetric distribution of helicity flux exists (Chen *et al.* 2003*b*), and we find that the distribution of the second-channel helicity flux is more symmetric than that of the first-channel helicity flux shown in figure 2(*b*). The discrepancies in flatness and distribution indicate that the second-channel helicity flux is more intermittent than the first-channel helicity flux, and the first-channel helicity flux is more intermittent than the energy flux, which is consistent with the conclusion in Chen *et al.* (2003*b*). The distribution regularities are similar at other scales, which are not shown for the sake of simplicity.

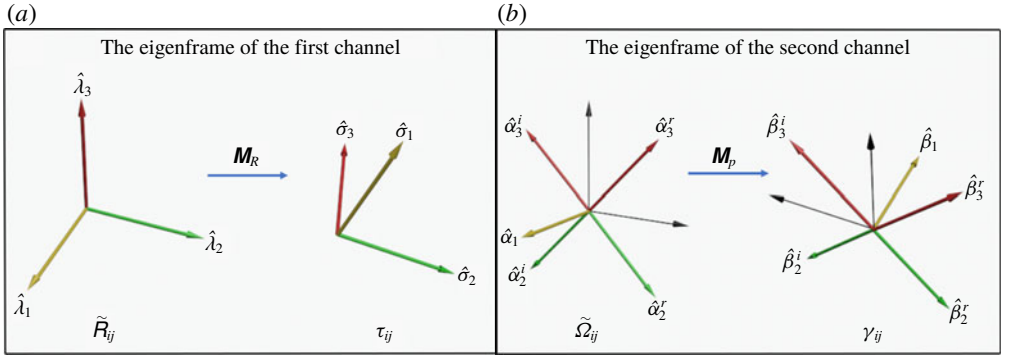

FIGURE 3. A schematic representing the relationships of the eigenframe of the first and second channels of helicity cascade; the superscripts r and i denote the real and imaginary parts of an eigenvector, respectively.

4.3. *Tensor geometry*

The turbulent cascade represented by the inner product of two tensors must address their relative alignment, and the tensor geometry in the turbulent cascade determines the efficiency of energy transfer (Ballouz & Ouellette 2018). The tensor geometries of the first- and second-channel helicity fluxes are totally different. The first channel consists of two real symmetric matrices, and the second channel consists of two real antisymmetric matrices. By eigen-decomposition, they can be expressed as

$$\Pi_{\Delta}^{H1} = -\mathrm{Tr}[\boldsymbol{\lambda} \boldsymbol{M}_R^{\mathrm{T}}(\phi, \theta, \psi) \boldsymbol{\Lambda} \boldsymbol{M}_R(\phi, \theta, \psi)], \tag{4.2}$$

$$\Pi_{\Delta}^{H2} = \mathrm{Tr}[\boldsymbol{\alpha} \boldsymbol{M}_P^{\mathrm{T}}(\phi, \theta, \psi) \boldsymbol{\beta} \boldsymbol{M}_P(\phi, \theta, \psi)], \tag{4.3}$$

where ϕ, θ and ψ are three ZYZ Euler angles (Shuster 1993; Ballouz & Ouellette 2018). In (4.2), $\boldsymbol{\lambda}$ and $\boldsymbol{\Lambda}$ are the diagonal matrices consisting of three eigenvalues of matrix $\boldsymbol{\tau}$ and $\widetilde{\boldsymbol{R}}$, respectively, and the $\boldsymbol{M}_R$ is the real rotation matrix from the second matrix $\widetilde{\boldsymbol{R}}$ to the first matrix $\boldsymbol{\tau}$. In (4.3), $\boldsymbol{\alpha}$ and $\boldsymbol{\beta}$ are the diagonal matrices including three eigenvalues of matrix $\boldsymbol{\gamma}$ and $\widetilde{\boldsymbol{\Omega}}$, respectively, and $\boldsymbol{M}_P$ is the plural rotation matrix from the second matrix $\widetilde{\boldsymbol{\Omega}}$ to the first matrix $\boldsymbol{\gamma}$. Here, we select one of the alternative rotation matrices as

$$\boldsymbol{M}_R = \begin{bmatrix} c\psi c\phi - s\psi c\theta s\phi & c\psi s\phi + s\psi c\theta c\phi & s\psi s\theta \\ -s\psi c\phi - c\psi c\theta s\phi & -s\psi s\phi + c\psi c\theta c\phi & c\psi s\theta \\ s\theta s\phi & -s\theta c\phi & c\theta \end{bmatrix},$$

where c and s denote cosine and sine, respectively.

The symmetric property of the two second-order tensors in the first channel determines that the eigenframes and rotation matrix are real, which is very similar to the tensor geometry of the energy cascade. The antisymmetric property of the tensors in the second channel determines that they are plural. According to the properties of the antisymmetric matrix, its three eigenvalues are zero and two conjugated pure imaginary numbers. For any eigenvector, its imaginary and real parts are isometric and orthogonal. Hence, we can easily determine the orthogonal and parallel geometric relationships between the eigenvectors' real and imaginary parts in figure 3. The imaginary and real parts of the second eigenvector can be uniquely merged into a

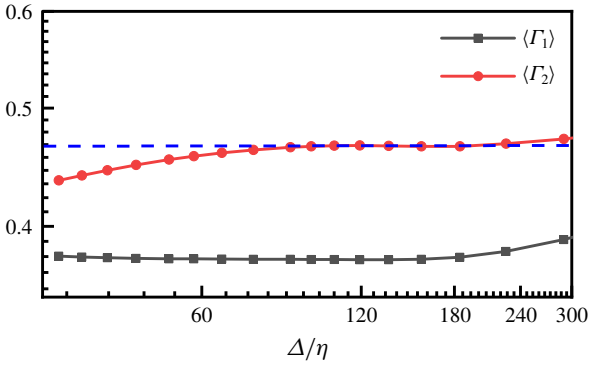

FIGURE 4. The average efficiencies of the first- and second-channel helicity fluxes as a function of Δ/η. The blue dashed line is a reference line with constant value 0.46.

new orthogonal vector, so it is in the third eigenvector. Therefore, the real rotation matrix $\boldsymbol{M}_R$ can also be applied equally to the rotation matrix of the second channel. For simplicity, the rotation matrix for the first and second channels is denoted by symbol $\boldsymbol{M}$.

The first- and second-channel helicity fluxes are expanded by the corresponding eigenvalues and rotation matrix as

$$\begin{aligned} -\Pi_\Delta^{H1} = {} & \lambda_1\Lambda_1[M_{11}^2 - M_{21}^2 - M_{12}^2 + M_{22}^2] + \lambda_3\Lambda_3[M_{33}^2 - M_{32}^2 - M_{23}^2 + M_{22}^2] \\ & + \lambda_1\Lambda_3[M_{31}^2 - M_{21}^2 - M_{32}^2 + M_{22}^2] + \lambda_3\Lambda_1[M_{13}^2 - M_{12}^2 - M_{23}^2 + M_{22}^2], \end{aligned} \tag{4.4}$$

where λ_1 and λ_3 are the first and third eigenvalues of matrix $\boldsymbol{\tau}$, and Λ_1 and Λ_3 are the first and third eigenvalues of matrix $\widetilde{\boldsymbol{R}}$. In addition, the incompressible condition has been considered in the above derivation, that is, $\lambda_1 + \lambda_2 + \lambda_3 = 0$. The divergence-free property of vorticity means that $\Lambda_1 + \Lambda_2 + \Lambda_3 = 0$. Nevertheless, the properties of an antisymmetric matrix lead to a more simplified expansion as follows:

$$\Pi_\Delta^{H2} = \alpha_3\beta_3[M_{33}^2 - M_{32}^2 - M_{23}^2 + M_{22}^2], \tag{4.5}$$

where α_3 is the third eigenvalue of matrix $\boldsymbol{\gamma}$, and β_3 is the third eigenvalue of matrix $\widetilde{\boldsymbol{\Omega}}$. The simpler rotation frame of the second channel of helicity flux involves lower-dimensional transformation, and this feature determines that the efficiency of helicity transfer through the second channel is naturally higher. Following the similar definition of the efficiency of energy cascade (Ballouz & Ouellette 2018), the efficiency of the helicity cascade through the first and second channels can be defined as

$$\Gamma_1 = \frac{\Pi^{H1}(\lambda_i, \Lambda_i, \phi, \theta, \psi)}{\Pi_{max}^{H1}(\lambda_i, \Lambda_i)}, \quad \Gamma_2 = \frac{\Pi^{H2}(\alpha_i, \beta_i, \phi, \theta, \psi)}{\Pi_{max}^{H2}(\alpha_i, \beta_i)}. \tag{4.6a,b}$$

The maximum of the first- and second-channel helicity fluxes can be achieved by seeking the optimal rotation matrix.

The averages of the helicity transfer efficiency through the first and second channels are numerically investigated in figure 4. Consistent with previous analysis, the helicity transfer efficiency through the second channel is higher, and the average efficiency in the inertial subrange is approximately 46 %. Besides, the average efficiency through

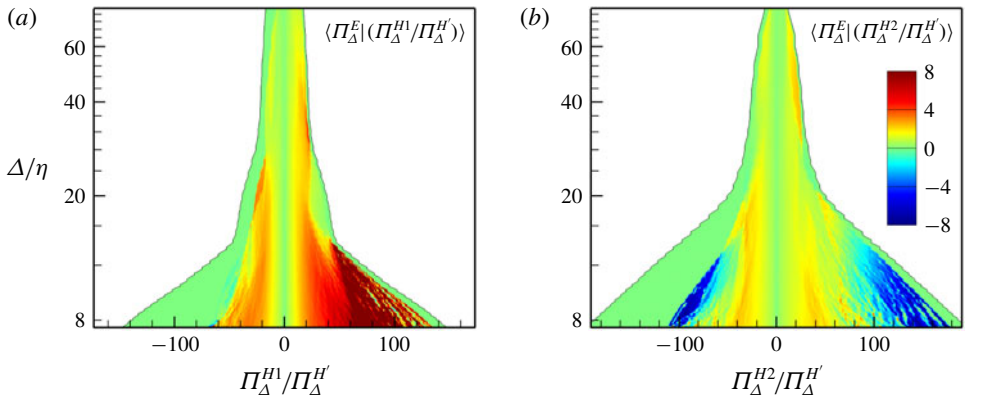

FIGURE 5. The local spatial average of energy flux conditioned on (*a*) the first-channel helicity flux Π_Δ^{H1} and (*b*) the second-channel helicity flux Π_Δ^{H2}. The longitudinal axis represents different filter widths, and $\Pi_\Delta^{H'}$ denotes the variance of the total helicity flux.

the second channel is also higher than the average efficiency of the energy cascade of 25 % in the inertial subrange (Ballouz & Ouellette 2018). Hence, we can infer that helicity tends to be reserved by the second channel, which means that more helicity is kept for transferring to the next scale. This second channel with higher transfer efficiency may serve as a new perspective for helicity transfer.

5. Roles of the dual channels in the energy cascade process

Relative to the triadic interactions of the same-chirality velocity (Biferale *et al.* 2012), the dual-channel helicity cascade proposed in this paper provides a new viewpoint for the mechanism of hindered or even inverse energy cascade. 'Vortex thinning' caused by the vortex stretching procedure as a physical mechanism for inverse energy cascade originates from the negative eddy viscosity theory (Kraichnan 1976), and is popularly applied to geophysics (Salmon 1998).

The conditional averaging method is always used to estimate the effects of certain factors on turbulent dynamos (Kovasznay, Kibens & Blackwelder 1970; Block *et al.* 2006). To evaluate the correlation between the energy flux and helicity flux at different length scales, we take the local spatial average of the energy flux conditioned on the first-channel and second-channel helicity fluxes in figure 5. The numerical results indicate that the ensemble average of the energy flux conditioned on the second channel is always smaller than that conditioned on the first channel, which is reflected as the lighter red or blue regions in figure 5(*b*). This means that the second channel of helicity cascade hinders the energy cascade at relatively large scales, and it can even reverse the direction of the energy cascade at small scales. In contrast, the first channel of helicity cascade promotes the forward energy flux, which is reflected by the scarlet regions in figure 5(*a*).

The local spatial averages of the energy flux conditioned on the absolute value of the ratio of the second and first channels of helicity cascade on four typical filter widths of relatively large scales are exhibited in figure 6. When the ratio is larger than one, we define that the second channel is dominant. The amplitudes of the energy flux are always smaller when the second channel is dominant. In addition, the amplitude of the energy flux also depends on the dominance degree of the second channel of

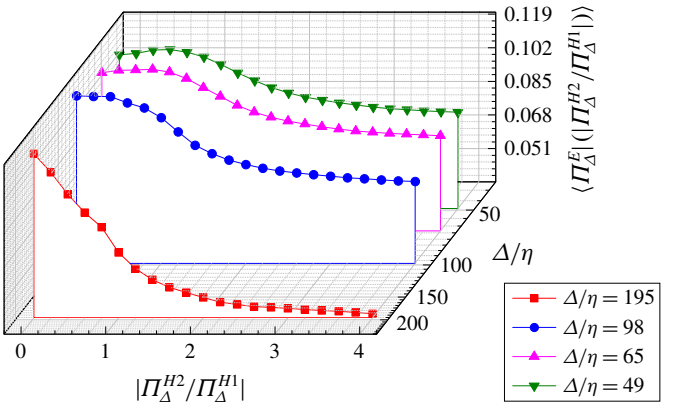

FIGURE 6. The local spatial average of energy flux conditioned on the absolute value of the ratio of the second channel and the first channel of helicity cascade on the typical filter widths ($\Delta/\eta = 49$, 65, 98 and 195).

helicity cascade. The above numerical evidence confirms again the hindering role of the second channel of helicity cascade in the inertial subrange. Based on the local conditional averaging method, we infer that the influence regularity of the second channel also applies to anisotropic turbulent flows. Therefore, we conclude that the second channel of helicity cascade provides a new perspective for controlling energy cascade. Under the influence of the second channel of helicity cascade, the small scales do not easily receive energy from large scales, and viscosity is not inclined to work well in near-dissipation regions. This conclusion is consistent with previous opinions that helicity can decrease the viscous dissipation of energy (Linkmann 2018).

6. Conclusions

This research reveals that a dual-channel helicity cascade exists in turbulent flows, and their properties are theoretically and numerically investigated in diverse aspects. The dynamics of these two channels are mainly dominated by vortex twisting and stretching, respectively. They behave differently in homogeneous and isotropic turbulence and anisotropic flows. The second channel of helicity cascade is more intermittent than the first channel. The tensor geometry of the second channel involves plural eigenframes and rotation matrix, which is more complicated than the tensor geometry of the first channel of helicity cascade and energy cascade. The first eigenvalue of the antisymmetric matrix is zero, which simplifies the helicity transfer procedure through the second channel and improves the transfer efficiency. The newly proposed second channel of helicity cascade can be recognized as a new promoting mechanism for the inverse energy cascade.

The dual-channel helicity cascade theory is a new perception of the helicity cascade in turbulent flows. When and where the second channel is dominant in a specific turbulent flow should be further verified. In natural phenomena, such as tornados and rainstorms, the role of the second channel needs to be further explored. In engineering turbulence control, the second channel of helicity cascade may serve as a practical scheme to improve fluid machinery efficiency. We infer that new turbulence models based on the dual-channel theory should be proposed to describe the turbulence process more precisely. More open issues exist, such as further analyses in compressible flows, and general anisotropic turbulent flows.

Acknowledgements

This work was supported by the National Natural Science Foundation of China (NSFC grant no. 91852203), and National Key Research and Development Program of China (2019YFA0405300, 2016YFA0401200). The authors thank the Johns Hopkins Turbulence Database (JHTDB) for providing publicly available turbulent channel flow data, and the National Supercomputer Center in Tianjin (NSCC-TJ) for providing computer time.

Declaration of interests

The authors report no conflict of interest

Appendix A. The derivation to prove the relation of the ensemble averages of the two helicity fluxes

Here, we provide a detailed derivation to prove the relation of the ensemble averages of the two helicity fluxes in both HIT and TCF.

The following identical equation exists:

$$\boldsymbol{\nabla}\cdot(\boldsymbol{a}\times\boldsymbol{b})=\boldsymbol{b}\cdot(\boldsymbol{\nabla}\times\boldsymbol{a})-\boldsymbol{a}\cdot(\boldsymbol{\nabla}\times\boldsymbol{b}), \tag{A 1}$$

where $\boldsymbol{a}$ and $\boldsymbol{b}$ are two arbitrary vectors. If we make an ensemble average of the left-hand side of the above identity, we can obtain the following result only when the three directions of flow are homogeneous:

$$\text{left-hand side}=\langle\boldsymbol{\nabla}\cdot(\boldsymbol{a}\times\boldsymbol{b})\rangle=0. \tag{A 2}$$

Hence, $\langle\boldsymbol{b}\cdot(\boldsymbol{\nabla}\times\boldsymbol{a})\rangle=\langle\boldsymbol{a}\cdot(\boldsymbol{\nabla}\times\boldsymbol{b})\rangle$.

If we define $a_i=u_i$ and $b_i=\partial\tau_{ij}/\partial x_j$, the first- and second-channel helicity fluxes could be expressed as

$$\begin{aligned}\langle\Pi_\Delta^{H1}\rangle &= -\left\langle\frac{\partial(\omega_i\tau_{ij})}{\partial x_j}\right\rangle+\left\langle\omega_i\frac{\partial\tau_{ij}}{\partial x_j}\right\rangle=\left\langle\omega_i\frac{\partial\tau_{ij}}{\partial x_j}\right\rangle=\left\langle\frac{\partial\tau_{ij}}{\partial x_j}\varepsilon_{ijk}\frac{\partial u_k}{\partial x_j}\right\rangle\\ &= \langle\boldsymbol{b}\cdot(\boldsymbol{\nabla}\times\boldsymbol{a})\rangle,\end{aligned} \tag{A 3}$$

$$\begin{aligned}\langle\Pi_\Delta^{H2}\rangle &= -\left\langle\frac{\partial(u_i\gamma_{ij})}{\partial x_j}\right\rangle+\left\langle u_i\frac{\partial\gamma_{ij}}{\partial x_j}\right\rangle=\left\langle u_i\frac{\partial\gamma_{ij}}{\partial x_j}\right\rangle=\left\langle u_i\varepsilon_{ijk}\frac{\partial(\partial\tau_{km}/\partial x_m)}{\partial x_j}\right\rangle\\ &= \langle\boldsymbol{a}\cdot(\boldsymbol{\nabla}\times\boldsymbol{b})\rangle.\end{aligned} \tag{A 4}$$

Hence, $\langle\Pi_\Delta^{H1}\rangle=\langle\Pi_\Delta^{H2}\rangle$ only in homogeneous and isotropic turbulence.

References

ALEXAKIS, A. 2017 Helically decomposed turbulence. *J. Fluid Mech.* **812**, 752–770.

ALEXAKIS, A. & BIFERALE, L. 2018 Cascades and transitions in turbulent flows. *Phys. Rep.* **767**, 1–101.

ALUIE, H. 2011 Compressible turbulence: the cascade and its locality. *Phys. Rev. Lett.* **106**, 174502.

ANDRE, J. C. & LESIEUR, M. 1977 Influence of helicity on the evolution of isotropic turbulence at high Reynolds number. *J. Fluid Mech.* **81**, 187–207.

BALLOUZ, J. G. & OUELLETTE, N. T. 2018 Tensor geometry in the turbulent cascade. *J. Fluid Mech.* **835**, 1048–1064.

BIFERALE, L. 2003 Shell models of energy cascade in turbulence. *Annu. Rev. Fluid Mech.* **35**, 441–468.

BIFERALE, L., MUSACCHIO, S. & TOSCHI, F. 2012 Inverse energy cascade in three-dimensional isotropic turbulence. *Phys. Rev. Lett.* **108**, 164501.

BIFERALE, L., MUSACCHIO, S. & TOSCHI, F. 2013 Split energy-helicity cascades in three-dimensional homogeneous and isotropic turbulence. *J. Fluid Mech.* **730**, 309–327.

BLOCK, D., TELIBAN, I., GREINER, F. & PIEL, A. 2006 Prospects and limitations of conditional averaging. *Phys. Scr.* **T122**, 25–33.

BRISSAUD, A. 1973 Helicity cascades in fully developed isotropic turbulence. *Phys. Fluids* **16**, 1366–1367.

BUZZICOTTI, M., LINKMANN, M., ALUIE, H., BIFERALE, L., BRASSEUR, J. & MENEVEAU, C. 2018 Effect of filter type on the statistics of energy transfer between resolved and subfilter scales from *a-priori* analysis of direct numerical simulations of isotropic turbulence. *J. Turbul.* **19**, 167–197.

CHEN, Q., CHEN, S. & EYINK, G. L. 2003*a* The joint cascade of energy and helicity in three-dimensional turbulence. *Phys. Fluids* **15**, 361–374.

CHEN, Q., CHEN, S., EYINK, G. L. & HOLM, D. D. 2003*b* Intermittency in the joint cascade of energy and helicity. *Phys. Rev. Lett.* **90**, 214503.

DUQUENNE, A. M., GUIRAUD, P. & BERTRAND, J. 1993 Swirl-induced improvement of turbulent mixing: laser study in a jet-stirred tubular reactor. *Chem. Engng Sci.* **48**, 3805–3812.

EYINK, G. L. 2006 Multi-scale gradient expansion of the turbulent stress tensor. *J. Fluid Mech.* **549**, 159–190.

FRISCH, U. 1995 *Turbulence: The Legacy of A. N. Kolmogorov*. Cambridge University Press.

GRAHAM, J., KANOV, K., YANG, X. I. A., LEE, M., MALAYA, N., LALESCU, C. C., BURNS, R., EYINK, G. L., SZALAY, A., MOSER, R. D. *et al.* 2016 A web services accessible database of turbulent channel flow and its use for testing a new integral wall model for LES. *J. Turbul.* **17**, 181–215.

KESSAR, M., PLUNIAN, F., STEPANOV, R. & BALARAC, G. 2015 Non-Kolmogorov cascade of helicity-driven turbulence. *Phys. Rev.* E **92**, 031004.

KOVASZNAY, L. S. G., KIBENS, V. & BLACKWELDER, R. F. 1970 Large-scale motion in the intermittent region of a turbulent boundary layer. *J. Fluid Mech.* **41**, 283–325.

KRAICHNAN, R. H. 1976 Eddy viscosity in two and three dimensions. *J. Atmos. Sci.* **33**, 1521–1536.

LILLY, D. K. 1986 The structure, energetic and propagation of rotating convective stroms. Part I. Energy exchange with the mean flow. *J. Atmos. Sci.* **43**, 113–125.

LINKMANN, M. 2018 Effects of helicity on dissipation in homogeneous box turbulence. *J. Fluid Mech.* **856**, 79–102.

MININNI, P. D. & POUQUET, A. 2009 Helicity cascades in rotating turbulence. *Phys. Rev.* E **79**, 026304.

MININNI, P. D. & POUQUET, A. 2010 Rotating helical turbulence. II. Intermittency, scale invariance, and structures. *Phys. Fluids* **22**, 035106.

MOFFATT, H. K. 1969 Degree of knottedness of tangled vortex lines. *J. Fluid Mech.* **35**, 117–129.

MOFFATT, H. K. 2014 Helicity and singular structures in fluid dynamics. *Proc. Natl Acad. Sci. USA* **111**, 3663–3670.

MOFFATT, H. K. 2017 Helicity-invariant even in a viscous fluid. *Science* **357**, 448–449.

MOFFATT, H. K. & DORMY, E. 2019 *Self-Exciting Fluid Dynamos*. Cambridge University Press.

MOFFATT, H. K. & TSINOBER, A. 1992 Helicity in laminar and turbulence flow. *Annu. Rev. Fluid Mech.* **24**, 281–312.

PELZ, R. B., YAKHOT, V., ORSZAG, S. A., SHTILMAN, L. & LEVICH, E. 1985 Velocity–vorticity patterns in turbulent flow. *Phys. Rev. Lett.* **54**, 2505–2508.

POUQUET, A., MARINO, R., MININNI, P. D. & ROSENBERG, D. 2017 Dual constant-flux energy cascades to both large scales and small scales. *Phys. Fluids* **29**, 111108.

SAHOO, G., ALEXAKIS, A. & BIFERALE, L. 2017 Discontinuous transition from direct to inverse cascade in three-dimensional turbulence. *Phys. Rev. Lett.* **118**, 164501.

SALMON, R. 1998 *Lectures on Geophysical Fluid Dynamics*. Oxford University Press.

SCHEELER, M. W., VAN REES, W. M., KEDIA, H., KLECKNER, D. & IRVINE, W. T. M. 2017 Complete measurement of helicity and its dynamics in vortex tubes. *Science* **357**, 487–491.

SHUSTER, M. D. 1993 A survey of attitude representations. *J. Astronaut. Sci.* **41**, 439–517.

STEPANOV, R., GOLBRAIKH, E., FRICK, P. & SHESTAKOV, A. 2015 Hindered energy cascade in highly helical isotropic turbulence. *Phys. Rev. Lett.* **115**, 234501.

SŁOMKA, J. & DUNKEL, J. 2017 Spontaneous mirror-symmetry breaking induces inverse energy cascade in 3D active fluids. *Proc. Natl Acad. Sci. USA* **114**, 2119–2124.

TEIMURAZOVA, A. S., STEPANOVA, R. A., VERMAB, M. K., BARMANB, S., KUMARB, A. & SADHUKHANB, S. 2018 Direct numerical simulation of homogeneous isotropic helical turbulence with the TARANG code. *J. Appl. Mech. Tech. Phys.* **59**, 1279–1287.

TEITELBAUM, T. & MININNI, P. D. 2009 Effect of helicity and rotation on the free decay of turbulent flows. *Phys. Rev. Lett.* **103**, 014501.

WALEFFE, F. 1992 The nature of triad interactions in homogeneous turbulence. *Phys. Fluids* A **4**, 350–363.

YU, C., HONG, R., XIAO, Z. & CHEN, S. 2013 Subgrid-scale eddy viscosity model for helical turbulence. *Phys. Fluids* **25**, 095101.